Curr Osteoporos Rep (2014) 12:465–474
DOI 10.1007/s11914-014-0233-0

IMAGING (T LANG AND F WEHRLI, SECTION EDITORS)

Micro- and Nano-CT for the Study of Bone Ultrastructure

Françoise Peyrin · Pei Dong · Alexandra Pacureanu · Max Langer

Published online: 8 October 2014

Abstract Micro-computed tomography (micro-CT)—a version of X-ray CT operating at high spatial resolution—has had a considerable success for the investigation of trabecular bone micro-architecture. Currently, there is a lot of interest in exploiting CT techniques at even higher spatial resolutions to assess bone tissue at the cellular scale. After recalling the basic principles of micro-CT, we review the different existing system, based on either standard X-ray tubes or synchrotron sources. Then, we present recent applications of micro- and nano-CT for the analysis of osteocyte lacunae and the lacunar-canalicular network. We also address the question of the quantification of bone ultrastructure to go beyond the sole visualization.

Keywords Computerized tomography · Synchrotron imaging · Micro-CT · Nano-CT · X-ray phase CT · Bone ultrastructure · Osteocyte lacunae · Canaliculi · Lacunar canalicular network · Bone quality · Lacunar density · Quantification

F. Peyrin · P. Dong · M. Langer
INSERM U1044, CREATIS, 69621 Villeurbanne, France

F. Peyrin · P. Dong · M. Langer
INSA-Lyon, 69621 Villeurbanne, France

F. Peyrin · P. Dong · M. Langer
CNRS UMR 5220, 69621 Villeurbanne, France

F. Peyrin · P. Dong · M. Langer
Université de Lyon, 69622 Lyon, France

F. Peyrin · P. Dong · M. Langer
Université Lyon 1, 69622 Villeurbanne, France

F. Peyrin (✉) · P. Dong · A. Pacureanu · M. Langer
European Synchrotron Radiation Facility, BP 220, 38043 Grenoble, Cedex, France
e-mail: peyrin@esrf.fr

Introduction

Bone fragility diseases such as osteoporosis are still the focus of active research to understand the mechanisms involved in bone loss and in bone failure. Although bone mass is an important determinant of bone strength, it is known not to be sole factor. According to Wolff's law, it has the property to adapt to the mechanical constraints to which it is subjected. Bone fragility is hypothesized to be the result of failed material or structural adaptations to mechanical stress [1, 2]. Bone adaptation results both from the bone modeling and remodeling processes. Thus, in response to loading, bone is expected to change its macro, micro, and nano structure.

Bone remodeling is achieved via mechanotransduction, a process in which the osteocyte system plays a major role [3–6]. Osteocytes are cells deeply buried in bone tissue communicating with each other through dendritic processes. Osteocytes and their processes are encapsulated within the so-called lacunar-canalicular network (LCN) [7]. Interstitial fluid flows circulating in the LCN are hypothesized to stimulate osteocytes. Microcracks could also interrupt cellular processes and participate in the transduction to trigger the repair process [8, 9]. For several years there has been a phenomenal interest in these bone cells qualified with expressions such as "the unrecognized side of bone tissue" or "can't hide forever" [10–14]. In addition to their participation in osteoclast recruitment and the initiation of bone remodeling, they have a role in maintaining mineral homeostasis. They secrete a number of factors, among which some are seen as potential therapeutic targets [15].

However, little quantitative data is available on the complex organization of the osteocyte network within osteons and interstitial tissue. This lack of data can be attributed to both a long-time lack of interest in the osteocyte system but also to the limited means for investigating this structure. Imaging the osteocyte system of the LCN is quite challenging because of its interior location within bone matrix, the small size of lacunae (a few micrometers) and canaliculi (100–700 nm in diameter), and the complexity of this network. The LCN forms a very dense network with several thousands of lacunae per mm^3 and hundreds of thousands of canaliculi per mm^3 constituting a tight meshwork within bone tissue.

Much knowledge on the osteocyte system comes from the early work of Marotti et al. [16, 17]. In 1979, these authors already characterized the three axis of the ellipsoidal shape of the osteocyte lacunae by using bone slices in different directions and determined that the major axis was parallel to the main orientation of the collagen fibers [18]. They later showed that osteocytes were located within loose cellular lamellae in comparison with dense acellular lamellae [19].

In most works, microscopic imaging techniques using either visible light, Scanning Electron Microscopy (SEM) or Transmission Electron Microscopy (TEM) have been used, the latter achieving the images at the highest spatial resolution. Nevertheless, most of these techniques provide only two-dimensional images making it difficult to obtain a complete understanding of the complex network. Several studies used stereology to extrapolate two-dimensional (2D) measurements to three-dimensional morphologic parameters [20]. However, such extrapolations are based on ideal shape models and can be biased due to inappropriate assumptions or to variations in the slicing direction. Thus, ideally the LCN should be investigated with a three-dimensional (3D) imaging modality providing sufficiently high spatial resolution. This was the conclusion of review paper from Schneider et al, which detailed the existing techniques and pointed out their limitations [21••].

Three-dimensional imaging of bone ultrastructure is currently a hot topic of research [22]. Confocal Laser Scanning Microscopy (CLSM) in which serial 2D optical microscopy images are acquired at consecutive layers by scanning the sample through the microscope focus has been the most widely used technique. It can reach high spatial resolution typically around 200 nm in the focal plane and approximately 450 nm in depth. Moreover, it can be coupled to a variety of fluorescence labels permitting to stain different cells [23]. This technique has, for instance, been used to obtain three-dimensional renderings of the osteocyte network in bone of animals [24, 25] and of women with and without fractures [26]. A number of recent studies investigating various properties of the osteocyte network are based on CLSM [27–29, 30•, 31]. Although the technique shows a potential, it still has some limitations, which includes decreased of contrast with depth and a maximum depth of about 100–150 μm due to the limited penetration and diffusion of visible light within hard tissues such as bone. In addition, the lower spatial resolution in the depth direction makes the images more difficult to analyze qualitatively and quantitatively. Other techniques such as coupling Focused Ion Beam (FIB) and SEM have been proposed but they have remained exploratory [32].

In contrast to light, X-rays easily penetrate through bone samples and X-ray imaging is particularly well suited for the analysis of bone at different scales [33]. At the micro structure scale, X-ray micro-CT has had considerable success for the analysis of trabecular bone, since it provides, nondestructively, a very large number of histology-like slices and direct 3D quantitative parameters of cancellous bone. It is also a technique of choice to investigate the Haversian and Volkmann porosity in cortical bone [34, 35]. While micro-CT systems used to image bone micro-structure are not directly adapted to investigate bone ultrastructure, nano-CT systems have been built for that purpose. Nevertheless, reaching the appropriate spatial resolution is a key issue to image ultrastructural features.

In this paper, we review how recent developments in X-ray CT systems are pushing CT imaging toward the cellular scale and beyond. In Section Two, after recalling the basis of X-ray CT, we introduce the advances in micro/nano-CT technology using either conventional X-ray tubes or X-rays extracted from synchrotron sources. In Section Three, we review the recent use of these systems to image the lacunar-canalicular network as well as properties of the bone extra cellular matrix.

CT Techniques

From X-Ray CT to X-Ray Nano-CT

The generic principle of X-ray CT is based on the combination of data acquisition and data processing to produce 2D images of the anatomy. Data acquisition is performed by rotating an X-ray source around the patient or sample and measuring the attenuation of X-rays as they pass through the body. The measures of attenuation do not directly provide the image, but a so-called sinogram. Then, by using a 2D tomographic reconstruction algorithm such as Filtered Back Projection (FBP), relying on an exact mathematical relationship relating the image to its sinogram, the CT image is obtained.

Clinical CT is used daily to image bone at the organ level but does not offer a sufficient spatial resolution to reveal bone microstructure. Since a gain in spatial resolution in CT is achieved at the cost of an increase of radiation exposure, this limits the possibility for in vivo imaging. High-resolution pQCT systems can now achieve spatial resolution as high as 150 micrometers but are restricted to peripheral bone (radius, tibia) [36].

It is technically possible to reach much higher spatial resolution for ex-vivo imaging. Experimental setups and commercial X-ray micro-CTs have been developed to image bone micro architecture [37]. Most systems use a cone beam X-Ray source associated with a two-dimensional detector. When the X-ray source is circularly rotated around the sample, a set of 2D radiographs at different view angles are recorded. The detector may be composed of a scintillator converting X-ray photons to light coupled to a 2D detector. The 3D image is generally reconstructed using the Feldkamp-David-Kress (FDK) algorithm, which generalizes the FBP algorithm [38]. This method is not exact as in the 2D case and can produce so-called cone beam artifacts. The errors increase with the divergence of the cone beam but remain low for cone angles smaller than 10°. They are more important in the top and bottom slices, which are sometimes excluded from the reconstruction.

Different machines with different characteristics in terms of X-ray voltage, current, and spatial resolution are available since it is not possible for a single micro-CT system to cover all ranges of spatial resolutions between 100 μm to 1 μm. The choice of spatial resolution is a key issue to obtain a satisfactory image of a given structure. Trabecular bone is generally imaged with voxel size between 5 μm and 20 μm, corresponding to fields of view of several centimeters (depending on the number of pixels of the detector). Imaging lacunae and canaliculi requires spatial resolutions at the micrometer or the nanometer scale.

A new generation of machines called X-Ray nano-CT has more recently been optimized to achieve ultra-high spatial resolutions. They generally use a nano focal spot source (<400 nm). Various vendors currently offer such machines. As an example, Bruker now offers a multi-scale X-ray nano-CT system (SkyScan2211) based on a cone beam design using an open pumped X-ray source with a voltage between 10 and 190 kV and a 14-bit detector (6 M pixels flat panel or 11 M pixels cooled CCD). The spatial resolution given by the vendor is 600 nm at 10 % modulation transfer function. However, due to the limited flux, the signal-to-noise ratio (SNR) may be low. The system can scan objects between 1 mm for the higher spatial resolutions (voxel size: 0.1 μm) up to 204 mm for lower spatial resolutions.

From Synchrotron X-Ray Micro-CT to Nano-CT

In parallel to desktop X-ray micro-CT, synchrotron radiation CT setups have also been developed to investigate bone micro architecture [39, 40]. Using synchrotron sources presents advantages for CT, especially for imaging samples up to the nanometer scale. Synchrotron sources offer a photon flux several orders of magnitude higher than that of conventional X-ray tubes. This property becomes particularly important for sub-micrometer spatial resolution imaging, thereby limiting scan times while achieving high SNR. They also permit use of monochromatic X-ray beams, avoiding the beam-hardening artifacts. The resulting image can then be considered as a map of the linear attenuation coefficient within the sample. Since this coefficient is related to the composition of the sample, it was used to estimate the degree of mineralization of bone in 3D [41]. During the past decade, SR micro-CT has been used for the simultaneous assessment of structure and mineralization in human or animal trabecular bone [42, 43]. Its application to cortical bone also permits quantification of the Haversian canal network and visualize osteons [34, 44, 45].

SR CT implemented at various synchrotron sources has been used at multiple spatial resolutions, ranging from 10 to 0.7 μm. The system developed on beamline ID19 at the ESRF is based on 3D parallel beam tomography and can provide images at nominal voxel size up to 0.2 μm [46]. The X-ray beam energy can typically be chosen in the range from 12 to 80 keV by using a double crystal monochromator. The 3D image is reconstructed from 1000 to 2000 radiographs, by the FBP algorithm performed on each slice. Setting a configuration at a given voxel size requires a number of adaptations in the beam size and flux as well as in the detection part, ie, the scintillator and eventually CCD detector.

Synchrotron sources also give access to phase contrast imaging. Propagation-based X-ray imaging is the simplest experimental implementation of phase contrast imaging and can be coupled to CT [47]. Acquisition of a phase CT image consists of recording one or several scans at different detector distances. The reconstruction algorithm includes a phase retrieval step prior to FBP reconstruction [48]. This technique provides a map of the so-called phase index decrement (δ), which is related to the electron density and yields higher sensitivity compared with the linear attenuation coefficient obtained in absorption CT.

Phase contrast imaging has been exploited to develop a magnified X-ray Nano-CT setup at the nano-imaging station ID22NI of the ESRF [49]. The beam is magnified by using a Kirkpatrick-Baez optical system. The X-ray energy can be set between 17 keV and 30 keV. Typically three or four scans of the sample recorded at different distances from the focal spot of the source are recorded. The system provides images with isotropic voxel sizes between 25 and 400 nm.

It is worth noting that the radiation exposure increases with the image spatial resolution and can reach 1 or several MGy [50, 51••]. Thus, if bone samples are analyzed with various techniques, very high spatial resolution X-ray imaging should be kept as the last step since it has an impact on bone mechanical properties [52].

X-Ray CT Imaging of Osteocyte Lacunae

Standard micro-CT systems used for the investigation of trabecular architecture have been reported to be limited for the visualization of osteocyte lacunae [53]. This was predictable since imaging osteocyte lacunae requires a spatial resolution better than 5 or 10 μm. Two initial studies have reported the use of X-ray nano-CT to examine the 3D morphology of osteocyte lacunae [54, 55]. In the first study, the authors analyzed bone samples from the calvaria and fibulae in adult mice by using both CLSM and nano-CT at voxel sizes of 390 nm (fibula) and 480 nm (calvaria) using the Skyscan 2011 system. The nano-CT images revealed that the lacunae at the two sites had different morphologies and were more elongated in fibula. In the second study, the authors analyzed cortical bone samples from the proximal tibia of three female patients with osteoarthritis, osteopenia, and osteopetrosis. They measured lacunar density, volume, surface area, and anisotropy ratio from nano-CT images (voxel size 580 nm) and observed significant differences in morphology. These two studies support the hypothesis that osteocyte lacunar morphology is affected by matrix strain due to different loading conditions but these studies remain limited in terms of numbers of samples and of analyzed lacunae. With the exception of these two studies, we are not aware of other work using desktop nano-CT for the analysis of lacunae. The limitations to diffusion of this technique could be related to the long image acquisition times and the lack of dedicated image analysis software to analyze the data.

At the same time, while the potential of SR CT for imaging bone at the cellular scale had been recognized early [56, 57], its use for the analysis of osteocyte lacunae in animal models or in humans has considerably increased during the last few years. SR micro-CT at SLS (Swiss Light Source) with a voxel size of 0.7 μm was first used to assess ultrastructural properties of cortical bone in two inbred strains of mice [58]. Recently, the same technique was used to analyze cortical bone porosity in a mouse model of osteogenesis imperfecta [59]. Among other differences, the authors found a higher lacunar density in osteogenesis imperfecta compared with a wild type. The cortical micro-porosities in rats treated with PTH or Alendronate were quantified using SR micro-CT at APS (Advance Photon Source) with a voxel size of 0.75 μm [60]. The lacunar porosity varied with treatment and was dependent on the location of the analyzed region within the cortex (endosteal, intracortical, periosteal). The lacunar properties in the tibial diaphysis in a control and immobilized model of rats were studied using SR micro-CT at Canadian Light Source with a voxel size of 2 μm [61]. The data revealed a significant decrease in lacunar density and lacunar volume in the immobilized group, demonstrating the effect of unloading on the lacunar properties. The different studies as well as lacunar densities and volumes are summarized in Table 1.

SR micro-CT also allowed the characterization of osteocyte lacunae in human cortical bone (Table 1). One sample from the femoral shaft of a 20 year old subject was imaged at the Advanced Photon Source, Argonne, IL, with a voxel size of 1.47 μm [62]. The authors analyzed the variations in lacunar density and volume with the distance from the Haversian canal in 11 osteons within a single image. Subsequently, the same group analyzed various samples taken in anterior, posterior, medial, and lateral regions within the same subject [63]. They reported variations in lacunar density depending on the site, more elongated and flattened lacunae in the anterior and posterior regions, but no significant differences in lacunar volume. The same imaging technique was used to analyze the femoral cortical bone in 30 women between 20 and 86 years [64••]. While there was no variation in lacunar density a significant reduction of lacunar volume was observed with age. In a recent study, we used SR micro-CT at 1.4 μm to analyze the statistical properties of lacunae in human femoral bone [65•]. The bone volume fraction was found to be significantly correlated to the lacunar density and other lacunar features.

To compare the results from various studies, it is important to know which parameters are extracted from the images and how they are calculated. After segmentation, counting the number of lacunae (Lc.N) and then assessing the lacunar density (Lc.N/TV or Lc.N/BV expressed in mm^{-3}) is straightforward. To assess lacunar shape, it is appropriate to use an ellipsoidal fit, which can be obtained by using the matrix of second order moments. Its 3 eigenvalues are related to axis lengths and its 3 eigenvectors provide the three ellipsoid axes, and thus, the orientation of the lacuna. Most work reported only the eigenvalues, which must not be confused with the lengths since the latter are actually proportional to the square root of the eigenvalues scaled by a factor $2\sqrt{5}$ [26, 65•]. To avoid confusion in units, it is recommended to provide the axis lengths directly. The lacunar ellipsoidal shape has been further characterized by various parameters involving ratios of eigenvalues or length axis. Since all these calculations are performed on each lacuna, the computing time may be an issue to process more than 10000 lacunae per image. An efficient calculation method allowing additional parameters such as the surface area, Euler number, and mean curvature was presented in [65•]. Such quantification provides not only the mean and standard deviation of all parameters but also its distribution within the examined ROI. Hannah et al reported a bimodal distribution in the lacunar volume in their initial study, but this observation was not confirmed in other work [62]. Very recently, a complete framework was described to extract even more parameters from such images [66••]. In the future, the comparison of results will certainly be simplified if the nomenclature and definition of parameters used to characterize lacunae is standardized.

Figure 1 shows SR CT images acquired at three different spatial resolutions. Figure 1a shows a region of interest in a slice in a human femoral cortical bone sample (voxel size 1.4 μm), Fig. 1b illustrates the osteocyte lacunae after segmentation, and Fig. 1c shows a colored map of the lacunae, coding the ratio of the two largest lengths of the lacunae.

X-Ray CT Imaging of Canaliculi

X-ray CT imaging of canaliculi making the junction between osteocyte lacunae is challenging due to the small diameter of

Table 1 Measurements of osteocyte lacunae parameters from desktop and SR nano-CT techniques. The number of samples, lacunar density, and average lacunar volumes are reported

Reference	Imaging tech	Location	Groups	Voxel size	Sample number	N.Lc (#)	Density type	Density (mm^{-3})	Volume (μm^3)
Vatsa et al, 2008	Desktop nano-CT	Mice	Fibular, Calvarial	390 nm, 480 nm	2	1790 993	-	-	-
van Hove et al, 2009	Desktop	Women proximal tibial	Osteoarthritis	580 nm	2	659	N.Lc/BV	21800	51.2
	Desktop nano-CT		Osteopenia	"	2	120.5	N.Lc/BV	8000	179.1
			Osteopetrosis	"	2	458.5	N.Lc/BV	15600	97.6
Britz et al, 2012	SR μCT	Rat tibia diaphysis	Control	2 μm	6	-	N.Lc/BV	63138	284
			Immobilized	"	6	-	N.Lc/BV	49641	209
Hannah et al, 2010	SR μCT	Man femoral diaphysis		1.47 μm	1	9807	N.Lc/TV	[40000–90000]	290
Carter et al, 2013	SR μCT	Man femoral diaphysis (A,P,M,L)		1.47 μm	13	-	N.Lc/BV	[26343–37521]	[378–409]
Carter et al, 2013	SR μCT	Woman femoral diaphysis (various ages)		1.47 μm	30	-	N.Lc/BV	23942	252
Dong et al, 2014	SR μCT	Human femoral mid-diaphysis		1.47 μm	13	12791	N.Lc/BV	20573	409.5
Mader et al, 2013	SR μCT	Mouse femoral mid-diaphysis	B6lit/lit, B6lit/+	1.4 μm	6	26063, 32514	N.Lc/BV	44800, 38500	317, 469
			C3Hlit/lit, C3Hlit/+	"	11	33799, 53287	N.Lc/BV	35700, 39000	378, 577
Schneider et al, 2007	SR μCT	Mouse femoral mid-diaphysis	B6-lit/lit	700 nm	1	-	N.Lc/TV	65865	200
			C3.B6-lit/lit	"	1	-		49879	269
Tommasini et al, 2012	SR μCT	Rat femoral diaphysis	Control	750 nm	6	-	N.Lc/TV	56470	266.0
			OVX, ALN, PTH	"	18	-	N.Lc/TV	[59510–63810]	[237.0–268.1]
Carriero et al, 2014	SR μCT	Mouse tibial and humeral mid-diaphysis	WT	700 nm	7	6471	N.Lc/TV	72981	375
			Oim	"	6	12347	N.Lc/TV	127365	363

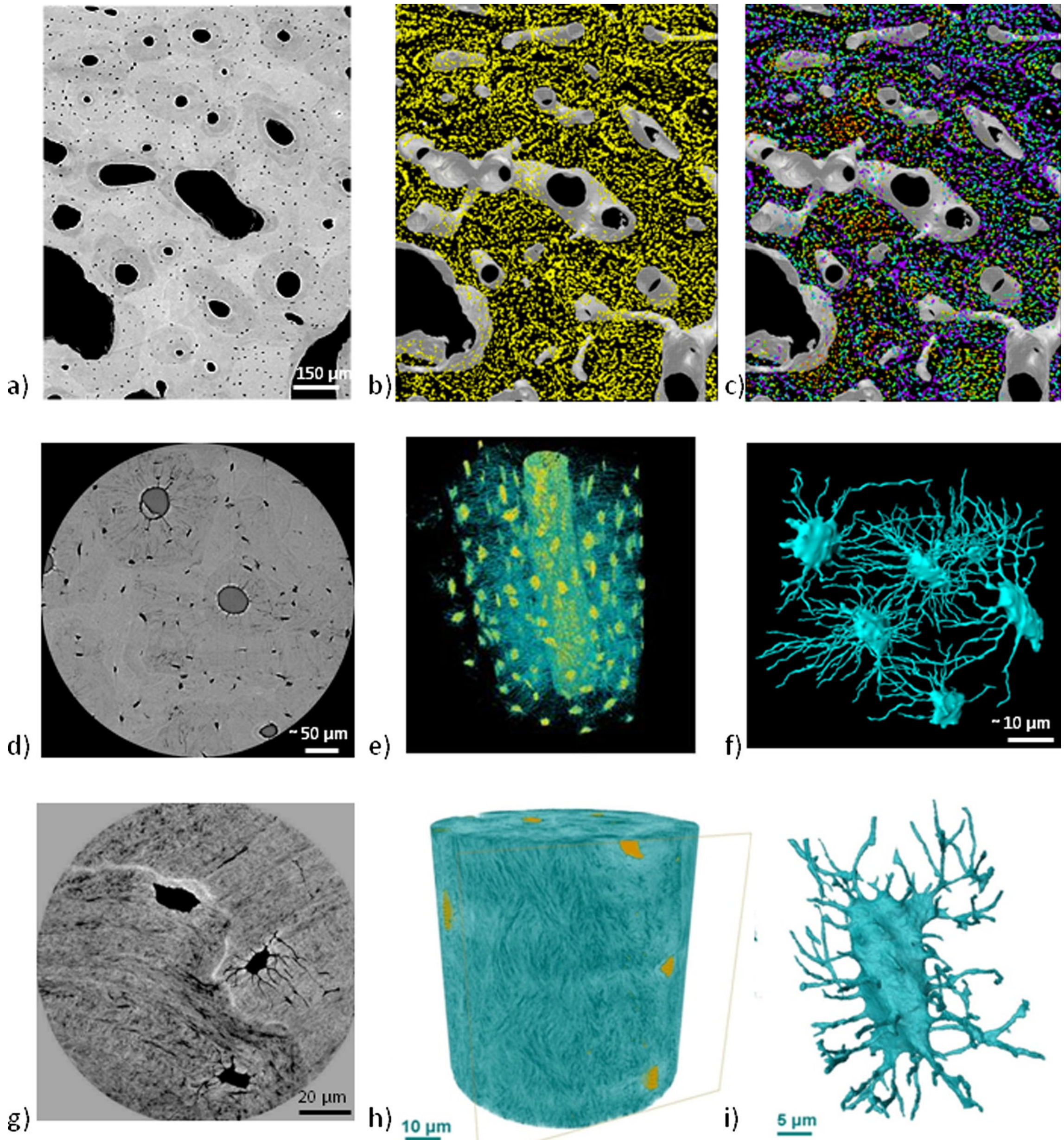

Fig. 1 Illustration of SR CT at different scales in human femoral bone samples: first row: voxel size 1.4 μm, (**a**) ROI in the original CT slice showing the Haversian porosity (black), the osteons (gray), the interstitial tissue (light gray), and osteocyte lacunae visible as small black dots, (**b**) 3D rendering of the osteocyte lacunae (yellow), (**c**) 3D rendering of the ratio of the two largest lengths of the osteocyte lacunae showing their anisotropy: second row: voxel size 300 nm, (**d**) ROI in the original CT slice showing osteons, osteocyte lacunae, and canaliculi, (**e**) 3D rendering of the lacunar-canalicular network around the top osteon of Fig. 1 (**d**) (lacunae in yellow, canaliculi in blue), (**f**) 3D display of 5 lacunae and their canaliculi segmented with the minimal path method presented in [69]: third row: voxel size 60 nm, (**g**) phase nano-CT slice showing a cement line (white) lacunae and canaliculi in black, (**h**) 3D rendering of the whole 3D image (lacunae in orange) where the collagen fibers form an apparent texture, (**i**) detail on one lacunae and its canaliculi

these structures. Up to now, standard X-ray source nano-CT has systems have not been successful to show these structures. While SR micro-CT has been reported to be a good candidate for the examination of canaliculi [21••], several works devoted to the analysis of lacunae using SR micro-CT outlined that the canaliculi were not visible even at submicrometer resolution [60].

The visualization of the LCN was demonstrated by using the parallel beam SR micro-CT setup at ESRF with a voxel size of 300 nm [51••]. This was only possible after optimization of the detector efficiency by coupling an adequate scintillator and a CCD camera to minimize the dose on the sample, responsible for cracks and motion artifacts. The advantage of this technique is that it provides 3D images of the LCN on

FOVs covering several osteons. However, since the pixel size was close to the canaliculi diameter, their segmentations was challenging and more sophisticated methods than simple thresholding had to be considered [67–69]. Figure 1d illustrates a ROI in a raw SR CT slice (voxel size: 300 nm) and Fig. 1e a 3D rendering of the LCN in an osteon. Figure 1f shows the segmentation of the LCN using a new method based on a minimal path approach preserving the continuity of the canaliculi [69].

A few images of the LCN at spatial resolutions between 40 and 60 nm were obtained based on experimental synchrotron techniques. In [70], the authors used rotated transmission X-ray microscopic images to obtain a 3D reconstruction of bone tissue at 40 nm, but the technique was limited to very small FOV (15–30 μm). The feasibility of visualizing one osteocyte lacunae surrounded by its canaliculi (spatial resolution 60 nm) was demonstrated by using ptychography, a scanning technique consisting of recording a sequence of overlapping diffraction patterns [71]. However, the long scan times and small FOVs restrict applications. Recently, a Talbot interferometer for phase CT imaging and edge-enhanced absorption CT were combined at SPring-8 in Japan to image the LCN in mouse bone [72]. Nevertheless, the complex acquisition procedure and long acquisition time hampers the practicality of the approach.

Our group used magnified phase nano CT at the ESRF to image the LCN in 3D at a voxel size of 60 nm [73••]. Compared with previous techniques, the FOV is larger (120 μm in each direction), which includes several lacunae. It provides details on the canaliculi organization and its branching structure but it also allows mapping of the density of the mineral tissue. The notable finding was that the collagen fibrils were visible as a textured pattern, the orientation of which was later analyzed [74••]. As an illustration, Fig. 1g illustrates a raw slice and Fig. 1h a 3D rendering of the whole sample, where the apparent orientation of collagen fibers is visible. Figure 1i shows a detailed rendering of a lacuna and its canaliculi. The same 3D phase nano-CT setup was later used to analyze the properties of the LCN in jaw bone samples arising from bisphosphonate-treated patients suffering osteonecrosis of the jaw [75].

Nano-CT, thus, permits a better assessment of bone tissue properties on the lamellar scale, including nanoporosity, quantification of mineralization and collagen fibers. Due to the recent findings at the lamellar length scale [76–78], this should open many perspectives for the understanding of bone fragility. The use of such images in modeling is also a promising area [79, 80].

Conclusions

The need for a three-dimensional assessment of bone ultrastructure has become more obvious. After the success of X-ray micro-CT for the quantification of bone microstructure, progress in X-ray nano-CT is expected. However, because of stringent requirements on X-ray flux at nanoscale, currently most studies at the ultrastructural level have been achieved using synchrotron sources CT setups. These systems can offer spatial resolution up to a few tens of nanometers with high SNR and fast scanning times. The feasibility of observing the 3D morphology of osteocyte lacunae, canaliculi, and even collagen fibers has been demonstrated.

After image acquisition, quantitative data have to be extracted from the images. Recently, automated methods have been proposed to calculate a number of 3D lacunae features on large data sets (more than 10,000 lacunae/sample). However, methods to quantify the complex canalicular networks have yet to be developed. In addition, it is worth noting that increasing spatial resolution puts a greater demand on data reconstruction and processing algorithms to analyze samples with meaningful field of view, given that the data size scales as the cube of sample size in on dimension.

Irrespective of the structural features to be quantified, the quality of the results strongly depends on image binarization. This problem is generally ignored and image segmentation performed by simple thresholding. This approach is often inadequate when the signal-to-noise ratio is low or when one dimension of the structure to be quantified is at the limit of the spatial resolution, as for instance for canaliculi. Thus, dedicated image segmentation methods have to be developed and evaluated, which is a major challenge since the ground truth may not be known.

To obtain information beyond structure, SR CT imaging also permits quantification of the density of the sample. At the microscale, this property has been exploited to map the degree of mineralization of bone and to discriminate osteons from interstitial tissue from absorption or phase imaging. At the ultrastructural level, phase nano-CT opens many perspectives to study peri-lacunar and peri-canalicular density and to observe the collagen fiber texture.

There are also some limitations to X-ray micro/nano CT techniques. First, so far, this technique only permits to visualize the pores rather than the cells or the osteocytic dendrites themselves. So the number of osteocyte lacunae can overestimate the number of osteocytes. However, many studies suggest that the analysis of osteocyte lacunae is a good surrogate of the osteocytes themselves provided that the percentage of empty lacunae remains approximately constant. Second, the accessibility of synchrotron sources is limited.

Nevertheless, X-ray nano-CT may provide reliable and innovative information on bone nano porosities, bone mineral, and extra cellular matrix at the cellular scale, which may be crucial to learn about the pathophysiological properties of bone tissue and more generally to gain a better understanding of bone mechanical properties.

Acknowledgments The images of bone samples were acquired at ESRF within the Long Term Project MD431. This work was performed within the framework of the LABEX PRIMES (ANR-11-LABX-0063) of Université de Lyon. The authors also want to thank Felix W. Wehrli for editing the manuscript.

Compliance with Ethics Guidelines

Conflict of Interest F. Peyrin, P. Dong, A. Pacureanu, and M. Langer declare that they have no conflicts of interest.

Human and Animal Rights and Informed Consent All studies by the authors involving animal and/or human subjects were performed after approval by the appropriate institutional review boards. When required, written informed consent was obtained from all participants.

References

Papers of particular interest, published recently, have been highlighted as:
- • Of importance
- •• Of major importance

1. Seeman E. Bone quality: the material and structural basis of bone strength. J Bone Miner Metab. 2008;26:1–8.
2. Compston J. Bone quality: what is it and how is it measured? Arq Bras Endocrinol Metab. 2006;50:579–85.
3. Nijweide PJ, Burger EH, Klein Nulend J. The Osteocyte [Internet]. Academic Press; 2002 [Accessed March 31, 2009]. Available at: http://dare.uva.nl/record/103838.
4. Knothe Tate ML, Adamson JR, Tami AE, Bauer TW. The osteocyte. Int J Biochem Cell Biol. 2004;36:1–8.
5. Klein-Nulend J, Bacabac RG, Mullender MG. Mechanobiology of bone tissue. Pathol Biol. 2005;53:576–80.
6. Bonewald LF. Mechanosensation and transduction in osteocytes. Bonekey Osteovision. 2006;3:7–15.
7. Burger EH, Klein-Nulend J. Mechanotransduction in bone—role of the lacuno-canalicular network. FASEB J. 1999;13:101–12.
8. Hazenberg JG, Freeley M, Foran E, Lee TC, Taylor D. Microdamage: a cell transducing mechanism based on ruptured osteocyte processes. J Biomech. 2006;39:2096–103.
9. Taylor D, Hazenberg JG, Lee TC. Living with cracks: damage and repair in human bone. Nat Mater. 2007;6:263–8.
10. Rochefort GY, Pallu S, Benhamou CL. Osteocyte: the unrecognized side of bone tissue. Osteoporos Int. 2010;21:1457–69.
11. Bonewald LF. The amazing osteocyte. J Bone Miner Res. 2011;26:229–38.
12. Bonewald LF, Kneissel M, Johnson M. Preface: the osteocyte. Bone. 2013;54:181.
13. Klein-Nulend J, Bakker AD, Bacabac RG, Vatsa A, Weinbaum S. Mechanosensation and transduction in osteocytes. Bone. 2013;54:182–90.
14. Kalajzic I, Matthews BG, Torreggiani E, Harris MA, Divieti Pajevic P, Harris SE. In vitro and in vivo approaches to study osteocyte biology. Bone. 2013;54:296–306.
15. Seeman E. Osteocytes—martyrs for integrity of bone strength. Osteoporos Int. 2006;17:1443–8.
16. Canè V, Marotti G, Volpi G, Zaffe D, Palazzini S, Remaggi F, et al. Size and density of osteocyte lacunae in different regions of long bones. Calcif Tissue Int. 1982;34:558–63.
17. Marotti G, Ferretti M, Remaggi F, Palumbo C. Quantitative evaluation on osteocyte canalicular density in human secondary osteons. Bone. 1995;16:125–8.
18. Marotti G. Osteocyte orientation in human lamellar bone and its relevance to the morphometry of periosteocytic lacunae. Metab Bone Dis Rel Res. 1979;1(4):325–33.
19. Marotti G, Ferretti M, Palumbo C. The problem of bone lamellation: an attempt to explain different proposed models. J Morphol. 2013;274:543–50.
20. Mullender MG, van der Meer DD, Huiskes R, Lips P. Osteocyte density changes in aging and osteoporosis. Bone. 1996;18:109–13.
21. •• Schneider P, Meier M, Wepf R, Müller R. Towards quantitative 3D imaging of the osteocyte lacuno-canalicular network. Bone. 2010;47:848–58. *Highlights the need and possible solutions for the investigation of the lacuno-canalicular network in 3D.*
22. Cardoso L, Fritton SP, Gailani G, Benalla M, Cowin SC. Advances in assessment of bone porosity, permeability and interstitial fluid flow. J Biomech. 2013;46:253–65.
23. Jones CW, Smolinski D, Keogh A, Kirk TB, Zheng MH. Confocal laser scanning microscopy in orthopaedic research. Prog Histochem Cytochem. 2005;40:1–71.
24. Sugawara Y, Kamioka H, Honjo T, Tezuka K, Takano-Yamamoto T. Three-dimensional reconstruction of chick calvarial osteocytes and their cell processes using confocal microscopy. Bone. 2005;36:877–83.
25. Kamioka H, Honjo T, Takano-Yamamoto T. A three-dimensional distribution of osteocyte processes revealed by the combination of confocal laser scanning microscopy and differential interference contrast microscopy. Bone. 2001;28:145–9.
26. McCreadie BR, Hollister SJ, Schaffler MB, Goldstein SA. Osteocyte lacuna size and shape in women with and without osteoporotic fracture. J Biomech. 2004;37:563–72.
27. Tonar Z, Khadang I, Fiala P, Nedorost L, Kochová P. Quantification of compact bone microporosities in the basal and alveolar portions of the human mandible using osteocyte lacunar density and area fraction of vascular canals. Ann Anat. 2011;193:211–9.
28. Sugawara Y, Ando R, Kamioka H, Ishihara Y, Honjo T, Kawanabe N, et al. The three-dimensional morphometry and cell-cell communication of the osteocyte network in chick and mouse embryonic calvaria. Calcif Tissue Int. 2011;88:416–24.
29. Kamioka H, Kameo Y, Imai Y, Bakker AD, Bacabac RG, Yamada N, et al. Microscale fluid flow analysis in a human osteocyte canaliculus using a realistic high-resolution image-based three-dimensional model. Integr Biol (Camb). 2012;4:1198–206.
30. • Kerschnitzki M, Kollmannsberger P, Burghammer M, Duda GN, Weinkamer R, Wagermaier W, et al. Architecture of the osteocyte network correlates with bone material quality. J Bone Miner Res. 2013;28:1837–45. *Highlights the role of osteocytes in bone homeostasis.*
31. Sharma D, Ciani C, Marin PAR, Levy JD, Doty SB, Fritton SP. Alterations in the osteocyte lacunar—canalicular microenvironment due to estrogen deficiency. Bone. 2012;51:488–97.
32. Schneider P, Meier M, Wepf R, Müller R. Serial FIB/SEM imaging for quantitative 3D assessment of the osteocyte lacuno-canalicular network. Bone. 2011;49:304–11.
33. Muller R. Hierarchical microimaging of bone structure and function. Nat Rev Rheumatol. 2009;5:373–81.
34. Bousson V, Peyrin F, Bergot C, Hausard M, Sautet A, Laredo JD. Cortical bone of the human femoral neck : three-dimensional appearance and porosity using synchrotron radiation. J Bone Miner Res. 2004;19:794–801.
35. Cooper DM, Thomas CD, Clement JG, Hallgrímsson B. Three-dimensional microcomputed tomography imaging of basic multicellular unit-related resorption spaces in human cortical bone. Anat Rec A: Discov Mol Cell Evol Biol. 2006;288:806–16.
36. Boutroy S, Bouxsein ML, Munoz F, Delmas PD. In vivo assessment of trabecular bone microarchitecture by high-resolution

peripheral quantitative computed tomography. J Clin Endocrinol Metab. 2005;90:6508–15.

37. Rüegsegger P, Koller B, Müller R. A microtomographic system for the nondestructive evaluation of bone architecture. Calcif Tissue Int. 1996;58:24–9.
38. Feldkamp LA, Davis LC, Kress JW. Practical cone-beam algorithm. J Opt Soc Am. 1984;1:612–9.
39. Engelke K, Graeff W, Meiss L, Hahn M, Delling G. High spatial resolution imaging of bone mineral using computed microtomography. Comparison with microradiography and undecalcified histologic sections. Investig Radiol. 1993;28:341–9.
40. Salome M, Peyrin F, Cloetens P, Odet C, Laval-Jeantet A, Baruchel J, et al. A synchrotron radiation microtomography system for the analysis of trabecular bone samples. Med Phys. 1999;26:2194–204.
41. Nuzzo S, Peyrin F, Cloetens P, Baruchel J, Boivin G. Quantification of the degree of mineralization of bone in three dimension using Synchrotron Radiation Microtomography. Med Phys. 2002;19:2672–81.
42. Nuzzo S, Peyrin F, Martín-Badosa E, Lafage-Proust MH, Boivin G. Quantitative analysis of mineral bone variation in 3D synchrotron radiation microtomography images. J Bone Miner Res. 2003;18:760–8.
43. Martin-Badosa E, Amblard D, Nuzzo S, Elmoutaouakkil A, Vico L, Peyrin F. Excised bone structures in mice: imaging at three-dimensional synchrotron radiation micro CT. Radiology. 2003;229:921–8.
44. Peter Z, Bousson V, Bergot C, Peyrin F. A constrained region growing approach based on watershed for the segmentation of low contrast structures in bone micro-CT. Pattern Recogn. 2008;41:2358–68.
45. Cooper DML, Erickson B, Peele AG, Hannah K, Thomas CDL, Clement JG. Visualization of 3D osteon morphology by synchrotron radiation micro-CT. J Anat. 2011;219:481–9.
46. Weitkamp T, Tafforeau P, Boller E, Cloetens P, Valade J-P, Bernard P, et al. Parallel-beam imaging at the ESRF beamline ID19: current status and plans for the future. Melbourne (Australia); 2010 [Accessed August 19, 2011]. p. 83–6. Available at: http://adsabs.harvard.edu/abs/2010AIPC.1234.83W.
47. Cloetens P, Pateyron M, Buffière JY, Peix G, Baruchel J, Peyrin F, et al. Observation of microstructure and damage in materials by phase sensitive radiography and tomography. J Appl Phys. 1997;81:5878–86.
48. Langer M, Cloetens P, Guigay JP, Peyrin F. Quantitative comparison of direct phase retrieval algorithms in in-line phase tomography. Med Phys. 2008;35:4556–66.
49. Mokso R, Cloetens P, Maire E, Ludwig W, Buffière J-Y. Nanoscale zoom tomography with hard x rays using Kirkpatrick-Baez optics. Appl Phys Lett. 2007;90:144104.
50. Barth HD, Launey ME, Macdowell AA, Ager III JW, Ritchie RO. On the effect of X-ray irradiation on the deformation and fracture behavior of human cortical bone. Bone. 2010;46:1475–85.
51.•• Pacureanu A, Langer M, Boller E, Tafforeau P, Peyrin F. Nanoscale imaging of the bone cell network with synchrotron X-ray tomography: optimization of acquisition setup. Med Phys. 2012;39:2229–38. *First report of synchrotron nano CT to image the lacuno-canalicular network in 3D and in entire osteons.*
52. Barth HD, Zimmermann EA, Schaible E, Tang SY, Alliston T, Ritchie RO. Characterization of the effects of x-ray irradiation on the hierarchical structure and mechanical properties of human cortical bone. Biomaterials. 2011;32:8892–904.
53. Draenert ME, Draenert AI, Forriol F, Cerler M, Kunzelmann K-H, Hickel R, et al. Value and limits of μ-CT for nondemineralized bone tissue processing. Microsc Res Tech. 2012;75:416–24.
54. Vatsa A, Breuls RG, Semeins CM, Salmon PL, Smit TH, Klein-Nulend J. Osteocyte morphology in fibula and calvaria—is there a role for mechanosensing? Bone. 2008;43:452–8.
55. Van Hove RP, Nolte PA, Vatsa A, Semeins CM, Salmon PL, Smit TH, et al. Osteocyte morphology in human tibiae of different bone pathologies with different bone mineral density—is there a role for mechanosensing? Bone. 2009;45:321–9.
56. Peyrin F, Salomé-Pateyron M, Cloetens P, Laval-Jeantet AM, Ritman E, Ruegsegger P. Micro-CT examinations of trabecular bone samples at different resolutions: 14, 7, and 2 micron level. Technol Health Care. 1998;6:391–401.
57. Peyrin F, Salome-Pateyron M, Nuzzo S, Cloetens P, Laval-Jeantet AM, Baruchel J. Perspectives in three-dimensional analysis of bone samples using synchrotron radiation microtomography. Cell Mol Biol. 2000;46:1089–102.
58. Schneider P, Stauber M, Voide R, Stampanoni M, Donahue LR, Müller R. Ultrastructural properties in cortical bone vary greatly in two inbred strains of mice as assessed by synchrotron light based micro- and nano-CT. J Bone Miner Res. 2007;22:1557–70.
59. Carriero A, Doube M, Vogt M, Busse B, Zustin J, Levchuk A, et al. Altered lacunar and vascular porosity in osteogenesis imperfecta mouse bone as revealed by synchrotron tomography contributes to bone fragility. Bone. 2014;61:116–24.
60. Tommasini SM, Trinward A, Acerbo AS, De Carlo F, Miller LM, Judex S. Changes in intracortical microporosities induced by pharmaceutical treatment of osteoporosis as detected by high resolution micro-CT. Bone. 2012;50:596–604.
61. Britz HM, Carter Y, Jokihaara J, Leppänen OV, Järvinen TLN, Belev G, et al. Prolonged unloading in growing rats reduces cortical osteocyte lacunar density and volume in the distal tibia. Bone. 2012;51:913–9.
62. Hannah KM, Thomas CDL, Clement JG, De Carlo F, Peele AG. Bimodal distribution of osteocyte lacunar size in the human femoral cortex as revealed by micro-CT. Bone. 2010;47:866–71.
63. Carter Y, Thomas CDL, Clement JG, Peele AG, Hannah K, Cooper DML. Variation in osteocyte lacunar morphology and density in the human femur—a synchrotron radiation micro-CT study. Bone. 2013;52:126–32.
64.•• Carter Y, Thomas CDL, Clement JG, Cooper DML. Femoral osteocyte lacunar density, volume and morphology in women across the lifespan. J Struct Biol. 2013;183:519–26. *Reports the 3D properties of osteocyte lacunae in women from 3D synchrotron micro-CT in a large age range.*
65.• Dong P, Haupert S, Hesse B, Langer M, Gouttenoire P-J, Bousson V, et al. 3D osteocyte lacunar morphometric properties and distributions in human femoral cortical bone using synchrotron radiation micro-CT images. Bone. 2014;60:172–85. *Reports a methodology for the 3D assessment of osteocyte lacunae.*
66.•• Mader KS, Schneider P, Müller R, Stampanoni M. A quantitative framework for the 3D characterization of the osteocyte lacunar system. Bone. 2013;57:142–54. *Reports a new methodology for the 3D assessment of osteocyte lacunae.*
67. Pacureanu A, Larrue A, Langer M, Olivier C, Muller C, Lafage-Proust M-H, et al. Adaptive filtering for enhancement of the osteocyte cell network in 3D microtomography images. IRBM. 2013;34:48–52.
68. Pacureanu A, Rollet J, Revol-Muller C, Buzuloiu V, Langer M, Peyrin F. Segmentation of 3D cellular networks from SR-micro-CT images. 2011 I.E. International Symposium on Biomedical Imaging: From Nano to Macro. IEEE; 2011. p. 1970–3.
69. Zuluaga MA, Orkisz M, Dong P, Pacureanu A, Gouttenoire P-J, Peyrin F. Bone canalicular network segmentation in 3D nano-CT images through geodesic voting and image tessellation. Phys Med Biol. 2014;59:2155.
70. Andrews JC, Almeida E, van der Meulen MCH, Alwood JS, Lee C, Liu Y, et al. Nanoscale X-ray microscopic imaging of mammalian mineralized tissue. Microsc Microanal. 2010;16:327–36.

71. Dierolf M, Menzel A, Thibault P, Schneider P, Kewish CM, Wepf R, et al. Ptychographic X-ray computed tomography at the nanoscale. Nature. 2010;467:436–9.
72. Nango N, Kubota S, Takeuchi A, Suzuki Y, Yashiro W, Momose A, et al. Talbot-defocus multi-scan tomography using the synchrotron X-ray microscope to study the lacuno-canalicular network in mouse bone. Biomed Opt Express. 2013;4:917–23.
73.•• Langer M, Pacureanu A, Suhonen H, Grimal Q, Cloetens P, Peyrin F. X-ray phase nanotomography resolves the 3D human bone ultrastructure. PLoS One. 2012;7:e35691. *First report of the lacuno-canalicular network using phase nano-CT at 60nm.*
74.•• Varga P, Pacureanu A, Langer M, Suhonen H, Hesse B, Grimal Q, et al. Investigation of the three-dimensional orientation of mineralized collagen fibrils in human lamellar bone using synchrotron X-ray phase nano-tomography. Acta Biomater. 2013;9:8118–27. *First analysis of collagen fibrils orientation from 3D phase nano-CT at 60 nm.*
75. Hesse B, Langer M, Varga P, Pacureanu A, Dong P, Schrof S, et al. Alterations of mass density and 3D osteocyte lacunar properties in bisphosphonate-related osteonecrotic human jaw bone, a synchrotron μCT study. PLoS One. 2014;9:e88481.
76. Granke M, Gourrier A, Rupin F, Raum K, Peyrin F, Burghammer M, et al. Microfibril orientation dominates the microelastic properties of human bone tissue at the lamellar length scale. PLoS One. 2013;8:e58043.
77. Reznikov N, Shahar R, Weiner S. Three-dimensional structure of human lamellar bone: the presence of two different materials and new insights into the hierarchical organization. Bone. 2014;59:93–104.
78. Schneider P, Voide R, Stampanoni M, Donahue LR, Müller R. The importance of the intracortical canal network for murine bone mechanics. Bone. 2013;53:120–8.
79. Verbruggen SW, Vaughan TJ, McNamara LM. Strain amplification in bone mechanobiology: a computational investigation of the in vivo mechanics of osteocytes. J R Soc Interface. 2012;9:2735–44.
80. Varga P, Hesse B, Langer M, Schrof S, Männicke N, Suhonen H, et al. Synchrotron X-ray phase nano-tomography-based analysis of the lacunar-canalicular network morphology and its relation to the strains experienced by osteocytes in situ as predicted by case-specific finite element analysis. Biomech Model Mechanobiol. 2014.